DOI: 10.13009/EUCASS2025-365
11TH EUROPEAN CONFERENCE FOR AERONAUTICS AND SPACE SCIENCES (EUCASS)

Design and Optimization of a Small Scale Solid Fuel Ramjet

Luca Armani [1,2]†, *Riccardo Nicoletti* [1], *Francesco Margani*[1,2],
Antonella Ingenito [1], *Shoesmith Ben* [1]
[1] *Department of Advanced Space Propulsion, Scuola di Ingegneria Aerospaziale-University of Rome La Sapienza, Italy ,*
[2] *GAUSS S.r.l., Italy,*
luca.armani@uniroma1.it · riccardo.nicoletti@uniroma1.it · francesco.margani@uniroma1.it
antonella.ingenito@uniroma1.it · ben.shoesmith@mail.mcgill.ca
†Corresponding author

Abstract

This paper presents the design and optimization of a small scale solid fuel ramjet (SFRJ) intended for testing at Mach 3.5 within a 30 cm-diameter test section of a supersonic wind tunnel. The design process begins with the optimization of a two-dimensional air intake, consisting of an external compression surface with multiple ramps. The ramp angles are calculated to achieve efficient compression while minimizing total pressure losses. To quantitatively assess the intake performance, a novel efficiency parameter is introduced, incorporating both total pressure losses and drag augmentation contribution. The optimized intake design is validated through Computational Fluid Dynamics (CFD) simulations to ensure accurate flowfield predictions. Building on the optimized intake, the combustion chamber is designed as a 2D configuration, incorporating a HTPB solid fuel. Finally, the overall ramjet design, including the intake, combustion chamber, and nozzle, is analyzed through CFD simulations under both cold-flow and reactive flow conditions. Aerodynamic performance and operational feasibility of the proposed design have been indeed validated showing promising performance for future high speed flight applications.

1. Introduction

Ramjet propulsion offers a compelling solution for high-speed atmospheric flight due to its mechanical simplicity, high thrust-to-weight ratio, and efficiency at supersonic velocities. Unlike turbojets, ramjets have no moving components, relying entirely on dynamic compression of incoming air and subsonic combustion to generate thrust.[1] These attributes make them ideal for future reusable launch systems.[1] Solid fuel ramjets (SFRJs) further enhance this simplicity by replacing complex liquid fuel systems with castable solid fuels such as Hydroxyl-Terminated Polybutadiene (HTPB). Despite their benefits in storability, structural compactness, and combustion stability,[2] SFRJs present unique challenges, including fuel regression control, flame holding, and the matching between intake dynamics and combustion processes.[2] Additionally, the transition to higher Mach numbers introduces increasingly significant aerodynamic and thermochemical constraints, particularly in terms of total pressure recovery and thermal loading.[3] The optimization of the intake and combustor geometry must therefore carefully balance shock-induced pressure losses with the need to provide favorable conditions for fuel pyrolysis and efficient mixing.

This study proposes a compact SFRJ model designed to operate at Mach 3.5, representative of a feasible test condition in ground-based facilities. Starting from the design of an external intake, a novel efficiency metric is introduced to evaluate trade-offs between aerodynamic drag and pressure recovery. The optimized intake configuration is then validated using CFD simulations. Subsequently, the combustion chamber and nozzle are designed to support the stable combustion of HTPB-based fuel. Simulations under both cold and reactive flow regimes confirm the feasibility and performance of the configuration. Fig. 1 illustrates the overall layout of the SFRJ. Key elements include the intake, isolator, and diffuser, which progressively compress the incoming flow, enabling stable fuel pyrolysis and ignition downstream. The combustion chamber is filled with HTPB fuel, which decomposes upon heating, releasing gaseous products that mix and react with the incoming air. Finally, a convergent-divergent nozzle accelerates the combustion products, converting thermal energy into directed thrust.

DOI: 10.13009/EUCASS2025-365

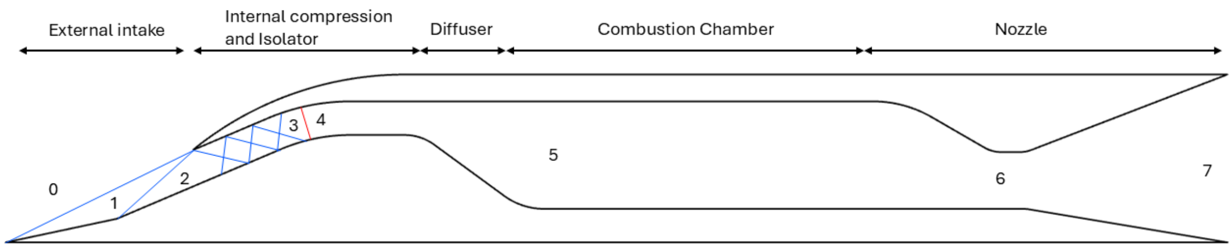

Figure 1: Ramjet Schematic

2. Intake Design

The intake of a ramjet engine plays a crucial role in ensuring efficient operation at high supersonic speeds. Its primary purpose is to decelerate and compress the incoming airflow before it enters the combustion chamber, without the use of moving parts. This process must be achieved with minimal total pressure losses and the design must produce the least possible amount of aerodynamic drag. To achieve this, the intake design must exploit shock waves and geometric features that control the behavior of supersonic flow. In particular, the use of oblique shocks generated by compression ramps allows for a gradual and efficient deceleration of the flow. These are typically followed by a normal shock or a series of weaker shocks, also known as shock train, to bring the flow to subsonic conditions, suitable for combustion. Downstream of the intake, the flow is expected to be subsonic, uniform, and sufficiently compressed, providing the necessary conditions for stable and efficient combustion. This includes achieving a high pressure recovery and avoiding flow separation or unsteadiness that could degrade engine performance.

For the present study, an external compression intake is selected. This configuration uses external compression, by means of a system of oblique shocks formed on external ramps. This design is particularly suited for high-speed applications, as it provides a good balance between total pressure recovery and structural complexity.

2.1 Ramps Optimization

To improve the intake performance, a parametric optimization study was carried out by varying the number of shock ramps and their respective turning angles. Configurations with one to three ramps and ramp angles ranging from 1° to 20° were analyzed. The core objective was to maximize pressure recovery while minimizing the total drag penalty associated with higher turning angles, particularly due to the increased inclination of the cowl.

The oblique shock relations, specifically the θ–β–M relations,[4] were employed to compute the flow deflection through each ramp and the resulting pressure rise across the shock system. For each configuration, the total pressure recovery ratio was calculated as:

$$\frac{P_c}{P_\infty} = \prod_{i=1}^{n} \left(\frac{P_i}{P_{i-1}} \right) \tag{1}$$

where n is the number of shock waves in the configuration and P_i is the static pressure after the i-th shock. However, maximizing pressure recovery alone is not sufficient. As the turning angle increases, the cowl becomes more inclined, leading to greater drag. To evaluate the overall intake efficiency, rather than maximizing pressure recovery alone, we introduce a fictitious net force $F_{\text{net}} = T - D$, where the thrust T is estimated as $T = C_f\, P_c\, A_t$, with C_f the thrust coefficient, P_c the static pressure at the end of the intake (which depends on pressure recovery), and A_t the throat area. The drag D is modelled by assuming a semi-spherical flow deflection over the cowl, giving

$$D = \tfrac{1}{2}\, \rho_\infty\, V^2\, (L_{\text{cowl}} \sin\alpha)\, C_d,$$

where ρ_∞ is the freestream density, V the freestream velocity, α the cowl inclination angle, $L_{\text{cowl}} \sin\alpha$ the projected surface area, and C_d the drag coefficient evaluated under the semi-spherical deflection assumption.[5]

Finally, to normalize the results and facilitate comparison across configurations, an efficiency index was defined:

$$\epsilon = \frac{F_{\text{net}} - F_{\text{net,min}}}{F_{\text{net,max}} - F_{\text{net,min}}} \tag{2}$$

This formulation indirectly promotes high pressure recovery since the static pressure P_c is embedded in the thrust term. The optimal intake configuration was selected as the one yielding the maximum ϵ value, thus balancing

DOI: 10.13009/EUCASS2025-365

compression efficiency and aerodynamic penalties. Since the present analysis investigates the variation of total pressure recovery (TPR) as a function of arbitrarily chosen ramp angles in a supersonic intake. According to the Oswatitsch criterion, maximum TPR is achieved when the normal part of all oblique shocks in the intake have equal strength and are followed by a terminal normal shock.[6,7] While this condition provides a theoretical optimum, practical configurations often deviate from it due to drag considerations. Increased ramp angles induce stronger initial oblique shocks, which decelerate the flow more rapidly. As a result, the terminal normal shock becomes weaker, leading to a higher overall pressure recovery. However, this benefit comes at the expense of higher total drag, primarily due to the larger frontal area of the intake. Therefore, the solutions obtained in this study reflect a trade-off between maximizing TPR and minimizing drag, deviating from the Oswatitsch-optimal configuration.

Shock Detachment Criterion In a supersonic flow over a wedge, the relationship between the flow deflection angle θ, the shock wave angle β, and the upstream Mach number M_1 is given by the θ–β–M relation:

$$\tan\theta = 2\cot\beta \cdot \frac{M_1^2 \sin^2\beta - 1}{M_1^2(\gamma + \cos 2\beta) + 2} \tag{3}$$

For a given M_1, this function has a maximum deflection angle $\theta_{\max}$ corresponding to a specific β. Beyond this point, the equation admits no real solutions for β, as the numerator of the fraction becomes negative and the inverse tangent argument becomes imaginary. This indicates that no attached oblique shock can turn the flow by an angle $\theta > \theta_{\max}$. As a result, the shock must detach from the wedge tip, forming a curved (detached) bow shock upstream of the body.

The results of this analysis demonstrate the existence of a limit to the ramp angles, with maximum efficiency achieved for values ranging between 10 and 20 degrees under the Mach conditions considered. In particular, the curve plotted in Figure 2a clearly indicates the presence of a maximum value. This behavior arises from the rapid increase in drag with the angle of incidence, surpassing a threshold beyond which the gain in pressure recovery is no longer sufficient to offset the drag penalty. In the single-ramp case, no shock detachment is observed. However, in the configurations shown in Figures 2b and 2c, regions of shock detachment are present most notably the dark blue area and the missing section of the graph in the three-ramp configuration. Another important observation concerns the maximum efficiency values. From one to three ramps, the peak efficiency increases, reaching values close to unity. At the same time, the angles corresponding to maximum efficiency decrease: for the single-ramp configuration, the peak occurs at 18 degrees; for the two-ramp configuration, it lies between 13 and 16 degrees; and for the three-ramp configuration, between 10 and 15 degrees, averaged across the ramps. Due to geometric constraints, the final design choice settled on a two-ramp configuration, with each ramp having an angle of 12 and 11 degrees, respectively, to prevent wall thicknesses from becoming too small and to fit the ramjet within a total height of 5 cm.

DOI: 10.13009/EUCASS2025-365

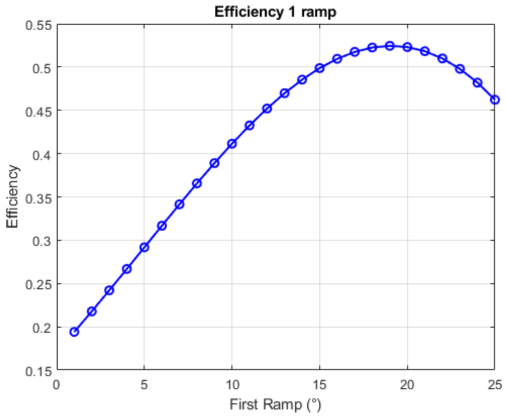

(a) Efficiency map for 1-ramp configuration

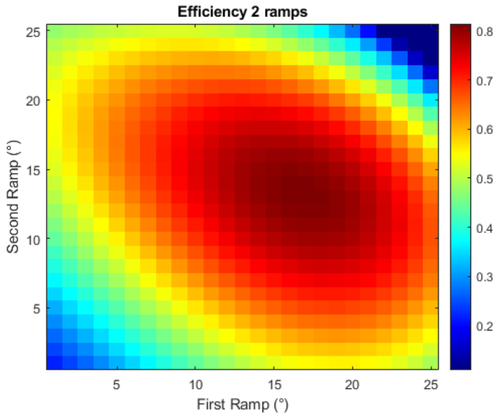

(b) Efficiency map for 2-ramp configuration

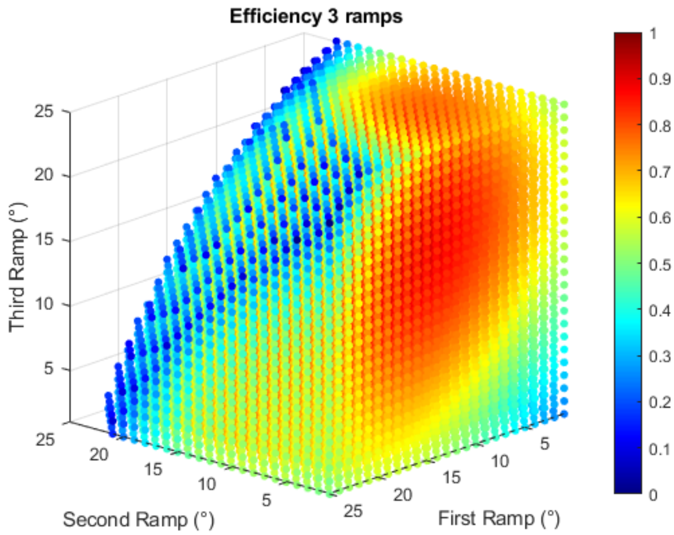

(c) Efficiency map for 3-ramp configuration

Figure 2: Comparison of efficiency maps for 1, 2, and 3 ramp intake configurations.

Isolator Design: The isolator, or constant-area throat section, plays a crucial role in ramjet intakes by hosting the terminal shock and ensuring stable subsonic diffusion downstream. Empirical studies suggest that the radius of curvature and by implication the isolator length should be no less than four times the isolator height to avoid choking and excessive losses due to wall pressure forces. This guideline is particularly relevant for maintaining supersonic flow and shock positioning near the isolator entrance.[8]

Post-Shock Deceleration and Flow Conditioning Following the oblique and normal shocks in the intake system, the flow is characterized by elevated pressure and temperature but subsonic velocity. To reduce the Mach number further down to the target value of $M \approx 0.2$, an isentropic compression section is introduced before the combustor. This deceleration phase plays a crucial role in increasing the static pressure and temperature of the chamber, enhancing mixing efficiency, and ensuring stable combustion. Since the flow is already subsonic, the divergent section does not lead to significant changes in the performance of the propulsion system. Therefore, a 40-degree angle was selected in order to reduce the overall length of the system.

3. Combustion Chamber and Nozzle

The sizing of the combustion chamber and nozzle in a ramjet propulsion system is a technically complex process that requires a careful balance between thermodynamic and aerodynamic principles, performance requirements, and structural constraints. The incoming air, after passing through the normal shock at the intake throat, is subsonic;

DOI: 10.13009/EUCASS2025-365

however, it must be further decelerated to ensure optimal combustion conditions. Specifically, it is desirable for the flow entering the combustion chamber to reach a Mach number below 0.2. This ensures sufficient residence time for mixing and reaction, it is also important to have a gradual increase of the area to avoid excessive pressure losses.

In the present study, a solid-fueled ramjet configuration is considered. The oxidizer is atmospheric air collected through the intake, while the propellant is a hybrid solid grain composed of Hydroxyl-Terminated Polybutadiene (HTPB). The solid grain is housed inside the combustion chamber and regresses upon exposure to the high-speed and high-temperature of the airflow, releasing fuel vapors that mix and react with the oxidizer.

3.1 Combustor Geometry and Mass Flow Constraints

The combustor geometry, including its length and cross-sectional area, must accommodate the required mass flow rates of air and fuel, while satisfying the oxidizer-to-fuel (O/F) ratio constraints for hybrid combustion, in this particular case, based on CEA code study, the value was selected to be 15, this value corresponds to an equivalence ratio (ϕ) of 1, indicating stoichiometric conditions. Assuming a fixed design thrust and specific impulse I_{sp}, corrected for ramjet, the fuel mass flow rate is obtained by:

$$\dot{m}_{\text{fuel}} = \frac{T}{I_{sp} \cdot g_0 - V_0} \tag{4}$$

where T is the net thrust, g_0 is gravitational acceleration, and V_0 is the flight velocity. Consequently, the oxidizer mass flow rate is defined as:

$$\dot{m}_{\text{ox}} = \text{O/F} \cdot \dot{m}_{\text{fuel}} \tag{5}$$

To ensure sufficient oxidizer availability, the intake area is sized accordingly. For a two dimensional intake configuration, the area is: $A_{\text{intake}} = h_{\text{intake}} \cdot b_{\text{intake}}$.

where h_{intake} is the fixed channel height (10mm), Fig. 1, stations 3 and 4, and b_{intake} is the variable intake width. The oxidizer mass flow rate is thus a function of post-shock flow properties:

$$\dot{m}_{\text{ox}} = M_2 \cdot h_{\text{intake}} \cdot b_{\text{intake}} \cdot \frac{P\sqrt{\gamma}}{\sqrt{RT}} \tag{6}$$

The equation is solved to determine the required b_{intake} that satisfies the equation for a given $\dot{m}_{\text{ox}}$.

3.2 Fuel Grain Optimization

The HTPB-paraffin grain regression is modeled using an empirical power-law formulation:

$$\dot{r}_b(t) = a\left(\frac{\dot{m}_{\text{air}}}{\pi r_{\text{int}}^2}\right)^n \tag{7}$$

where a and n are empirical coefficients, and r_{int} is the inner port radius of the fuel grain, Fig. 3b. The instantaneous fuel mass flow rate is computed as:

$$\dot{m}_{\text{fuel}}(t) = \rho_p \cdot \dot{r}_b(t) \cdot A_b(t) \tag{8}$$

with ρ_p the fuel density and $A_b(t)$ the time-dependent burning surface area. An optimization routine iteratively adjusts the initial grain geometry (length and inner radius) to minimize the deviation from a reference $\dot{m}_{\text{fuel}}$ and ensure temporal stability of the combustion process. Final optimized values for the grain length and radius are used to define the overall length of the combustion chamber.

3.3 Nozzle Design and Expansion Considerations

The nozzle is designed to accelerate the combustion products and generate thrust by means of a controlled expansion process, with the aim of achieving fully adapted flow conditions at the exit. At the design condition the stagnation pressure leaving the combustion chamber P_{cc}, is known and the isoentropic relation allows us to find the corresponding Mach number:

$$P_{\text{exit}} = P_{cc} \cdot \left(1 + \frac{\gamma - 1}{2} M_{\text{e}}^2\right)^{-\frac{\gamma}{\gamma-1}} \tag{9}$$

DOI: 10.13009/EUCASS2025-365

The nozzle exit area is then found using the area Mach relation[4] :

$$\frac{1}{M_e}\left(\frac{2}{\gamma+1}\right)^{\frac{\gamma+1}{2(\gamma-1)}}\left(1+\frac{\gamma-1}{2}M_e^2\right)^{\frac{\gamma+1}{2(\gamma-1)}}=\frac{A_{\mathrm{exit}}}{A_t} \tag{10}$$

In cases where geometric constraints prevent achieving the ideal expansion ratio, the nozzle may be under-expanded. While this condition leads to minor efficiency losses, it can still be acceptable particularly in wind tunnel test campaigns as it simplifies the design while maintaining overall system feasibility.

Undersized Nozzle Throat It is essential to ensure that the intake and nozzle are properly balanced to maintain steady-state operation. If the nozzle throat is undersized relative to the intake, air may accumulate in the combustion chamber, increasing the static pressure and pushing the normal shock upstream, potentially outside the isolator. This causes intake unstart and oscillatory flow behavior. Therefore, the mass flow rates must satisfy:

$$\dot{m}_{\mathrm{intake}}=\dot{m}_{\mathrm{nozzle}}^{\mathrm{max}} \tag{11}$$

To achieve this, CFD simulations were used to refine the geometry, validate flow stability, and ensure that the pressure and Mach profiles matched the theoretical design under cold-flow conditions.

3.4 Final Geometry

The final cold flow and reactive flow configurations are shown in Figures 3a and 3b. These represent the converged geometrical solutions obtained through the iterative design process. In the following sections, the CFD results will be presented, along with the performance issues that emerged and the design improvements that were necessary to achieve the final stable configurations. Based on the analytical calculations of the previous chapters Tab. 1 and Tab. 2 are here reported.

Table 1: Values of flow variables at ground condition

Condition	P_{total} [Pa]	P_{static} [Pa]	T_{static} [K]	M
Initial condition	7.70×10^6	1.01×10^5	290.00	3.50
After first oblique shock	7.04×10^6	2.65×10^5	392.05	2.79
After second oblique shock	6.76×10^6	5.56×10^5	490.04	2.28
After normal shock	3.99×10^6	3.28×10^6	946.03	0.54
Combustion chamber	3.99×10^6	3.89×10^6	992.56	0.20

Table 2: Values of flow variables at 15.000m of altitude

Condition	P_{total} [Pa]	P_{static} [Pa]	T_{static} [K]	M
Initial condition	9.18×10^5	1.20×10^4	216.00	3.50
After first oblique shock	8.39×10^5	3.16×10^4	292.01	2.79
After second oblique shock	8.06×10^5	6.63×10^4	365.00	2.28
After normal shock	4.76×10^5	3.92×10^5	704.63	0.54
Combustion chamber	4.76×10^5	4.63×10^5	739.29	0.20

DOI: 10.13009/EUCASS2025-365

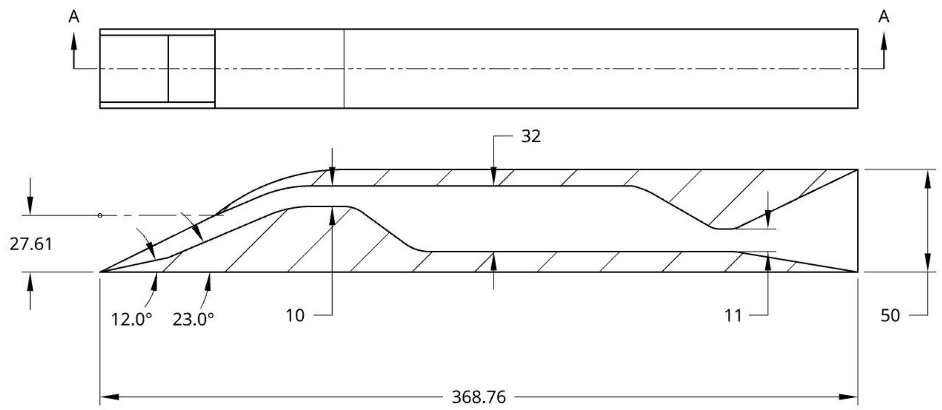

(a) Design Cold Final

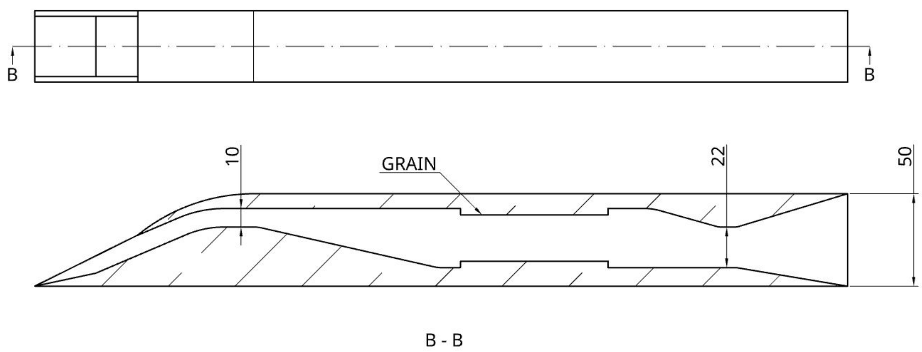

(b) Design Reactive Final

Figure 3: Comparison between cold-flow and reactive-flow final designs.

4. CFD Analysis

The initial CFD analysis was dedicated to evaluating the intake performance, neglecting the effects of the combustion chamber and nozzle. CFD simulations were performed using a density based solver with energy equations enabled and a CFL number of 0.3. The $k\omega$-SST turbulence model was selected for its accuracy in capturing shock boundary layer interactions and flow separation. Spatial discretization was analysed using second order upwind schemes to ensure numerical accuracy across the domain. Boundary conditions include a pressure farfield, back pressure outlet, and adiabatic walls. The farfield was set to Mach 3.5, with a static temperature of 290K and static pressure of 101,000Pa, while the back pressure at the outlet was fixed at 500,000Pa and 900K to emulate combustion chamber conditions. As shown in Figure 4a, the incoming flow is correctly decelerated by a system of oblique shocks forming at the expected locations and angles. The first shock reduces the Mach number to approximately 2.8, the second to 2.3, consistent with the theoretical value reported in Table 1. Figure 4b confirms the corresponding increase in static pressure, with the shock induced jumps is clearly visible, the increase in pressure fundamental to improve the combustion efficiency. Figure 4c displays the rise in static temperature across the shock system, further indicating proper thermodynamic behavior. Reaching a combustion chamber temperature of almost 800K. Lastly, Figure 4d illustrates total pressure losses, which remain contained and localized around shock interactions. Here it is possible to see that the presence of a fully developed normal shock cannot yet be observed. Considering an upstream Mach number greater than 2, significant SBLI effects become evident, and the total pressure is still higher than expected. This makes it difficult to evaluate the correct pressure recovery. Nevertheless, a terminal shock is present as part of a shock system that allows the transition from supersonic to subsonic flow. The overall agreement between numerical and analytical results confirms that the shock sequence, two oblique shocks followed by a normal shock, is present, creating the subsonic conditions necessary for efficient combustion downstream.

DOI: 10.13009/EUCASS2025-365

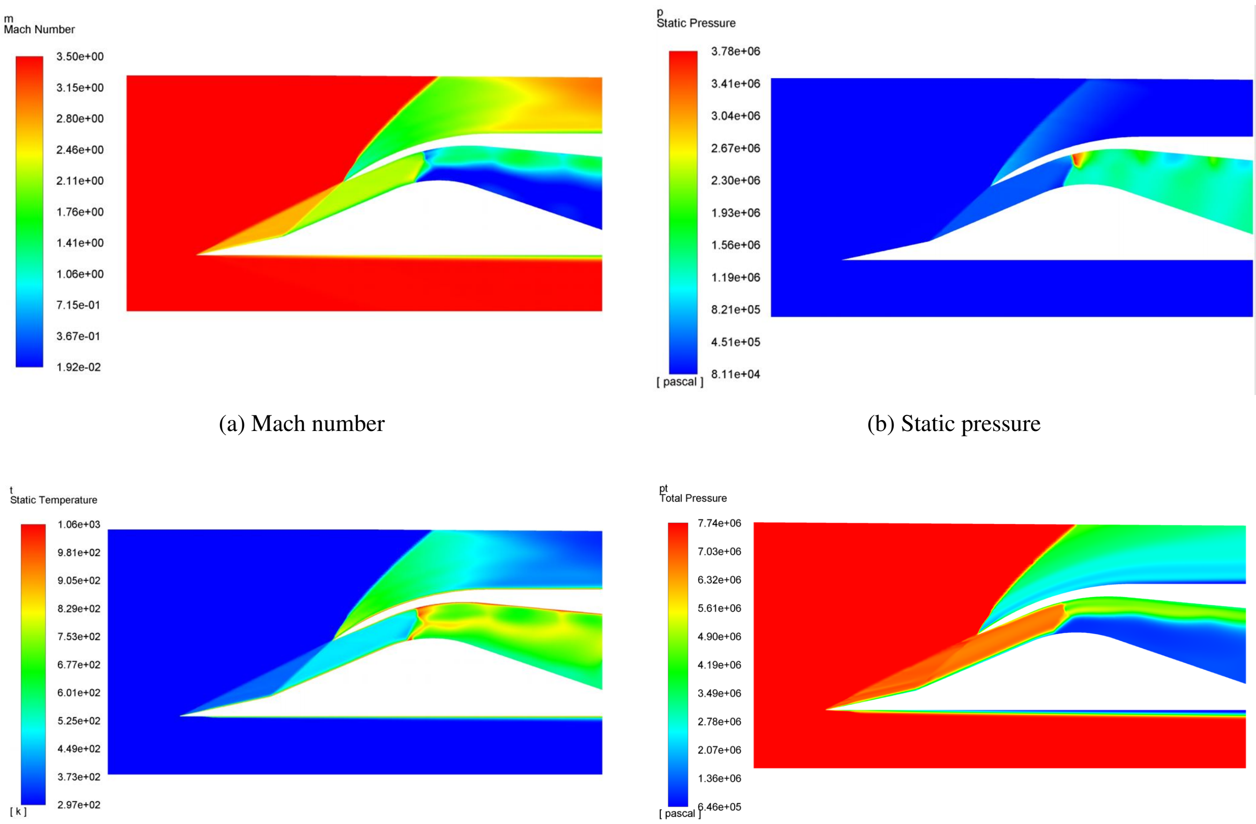

(a) Mach number

(b) Static pressure

(c) Static temperature

(d) Total pressure

Figure 4: Flow properties at the intake section

The main flow characteristics are summarized in Tab. 3 and results in good agreement with the predicted values of Tab.1. These quantities have been computed as mean values along the centerline.

Table 3: CFD results

Condition	**P_{total} [Pa]**	**P_{static} [Pa]**	**T_{static} [K]**	**M**
Initial condition	7.74×10^6	1.01×10^5	290.00	3.50
After first oblique shock	7.1×10^6	3.16×10^4	375.10	2.79
After second oblique shock	8.06×10^5	5.02×10^4	501.00	2.28
After normal shock	4.76×10^5	1.42×10^6	702.63	0.50
Combustion chamber	4.76×10^5	1.54×10^6	739.29	0.20

4.1 Buzz Instability

After confirming that the intake behavior matched the analytical results, the analysis progressed to the full model, incorporating both the combustion chamber and the nozzle. A particularly relevant observation from the CFD results, as already mentioned in section 3.3, was the negative impact of an undersized nozzle throat relative to the intake throat area. In one of the tested designs, the nozzle throat was smaller than the intake throat, which led to a significant increase in static pressure within the combustion chamber. This phenomenon severely affected the stability of the ramjet operation.

This instability is directly correlated with the pressure recovery of the intake. If the back pressure exceeds a critical value determined by the intake geometry and its area ratios, the shock can no longer remain stable inside the isolator and is pushed upstream into the intake. This is a fundamental constraint arising from mass conservation and the pressure and area relationships in compressible flow.

In this context, for a given intake throat area, there exists a maximum allowable static pressure in the combustion chamber beyond which stable supersonic flow cannot be sustained. If the nozzle throat is too small, it becomes a bottleneck: the mass flow rate through the nozzle cannot match the mass flow rate entering the intake:

DOI: 10.13009/EUCASS2025-365

$$\dot{m}_{\text{intake}} > \dot{m}_{\text{nozzle}} \tag{12}$$

As a result the static pressure increases beyond the limit. This triggers the displacement of the normal shock upstream into the intake ramps, disrupting the intake compression process. The phenomenon manifests as a *self-sustained oscillatory instability* known as *intake buzz*, where the shock repeatedly moves in and out of the intake. Based on the transient CFD analysis shown in Figure 5, the author estimated an oscillation period of approximately 3 milliseconds. This extremely short timescale explains why the phenomenon can manifest as an audible high frequency buzz.

The evolution of the intake unstart mechanism can be analyzed at key instants in the transient CFD simulation:

- **At 0.0 ms:** No shocks are yet established. Due to the low static pressure in the combustion chamber, the incoming supersonic flow can freely propagate through the isolator and into the combustion chamber without encountering significant resistance.

- **At 1.0 ms:** The first oblique shock has formed, causing a localized increase in pressure downstream of the shock. As a result, the static pressure in the combustion chamber rises.

- **At 1.4 ms:** The second oblique shock is now also formed, further compressing the flow and significantly increasing the pressure in the combustion chamber. At this stage, the nozzle throat, having a lower mass flow capacity than the primary contributes to a rapid pressure build up downstream.

- **At 1.6 ms:** The increasing backpressure destabilizes the intake flow. The normal shock is not yet stabilized and begins to move upstream, indicating the onset of unstart conditions.

- **At 1.8 ms:** The normal shock has been fully expelled from the isolator and propagates upstream. This is a consequence of the elevated combustion chamber pressure exceeding the critical backpressure the intake can sustain.

- **At 3.0 ms:** The total pressure increase within the combustion chamber rises the mass flow rate through the nozzle and the second throat begins to relieve the accumulated pressure, allowing the static pressure in the combustion chamber to decrease. The system gradually returns to its initial state, and the cycle begins again.

To prevent this instability, the nozzle throat must be correctly sized so that the mass flow rate through the nozzle can match the intake mass flow rate under design conditions, ensuring the combustion chamber pressure remains below the Kantrowitz limit. According to compressible flow theory, this translates into a constraint on the area ratio between the intake and nozzle throats, which must respect the balance of total pressures:

$$\frac{A_{\text{nozzle}}}{A_{\text{intake}}} \geq \frac{P_{t,\text{nozzle}}}{P_{t,\text{intake}}} \tag{13}$$

This relation highlights how sensitive the stability of the ramjet is to the sizing of the nozzle throat. Undersizing it even slightly can result in exceeding the critical back pressure, triggering buzz and leading to inefficient or failed operation.

DOI: 10.13009/EUCASS2025-365

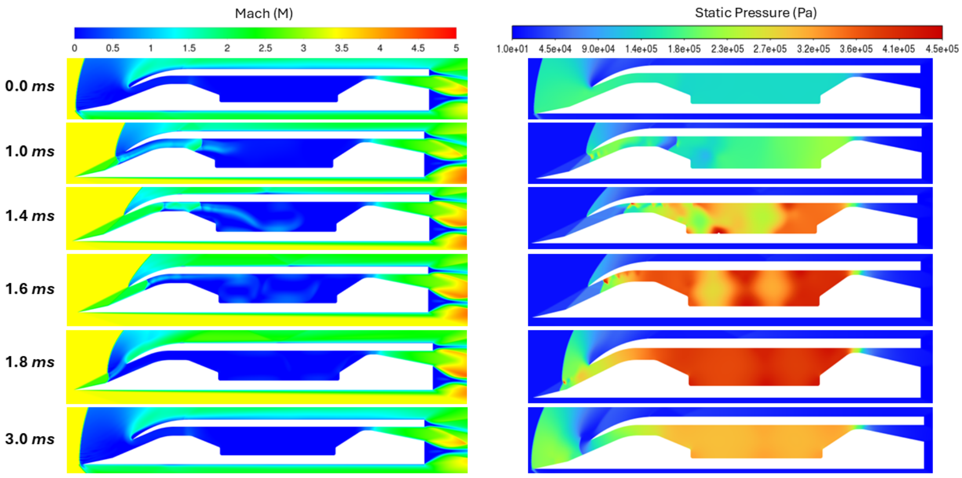

Figure 5: Buzz instability: Mach and Static Pressure contours

4.2 Cold Flow

In order to avoid the problem of buzz instability and allow the intake to operate without spilling mass flow the nozzle throat was increased by 10%.[9] The analysis setup remained the same as described in Section 4. However, the boundary conditions were revised to reflect flight conditions at an altitude of 15,000 m, as reported in Table 2. The results showed successful starting and stable conditions within the isolator and combustion chamber, indicating that the second throat was properly sized. As shown in Fig. 6a, the Mach number in the combustion chamber is more uniform compared to previous cases. Similarly, the temperature distribution in Fig. 6d is more homogeneous and reaches 720 K. This matches the analytical values in Table 2. The slightly lower temperature and static pressure values are a direct consequence of the increased second throat area, which is nonetheless essential for maintaining flow stability. Finally, Fig. 6c shows that the major total pressure loss is caused by the normal shock. However, the presence of two oblique shocks helps reduce its intensity, thereby improving the overall efficiency.

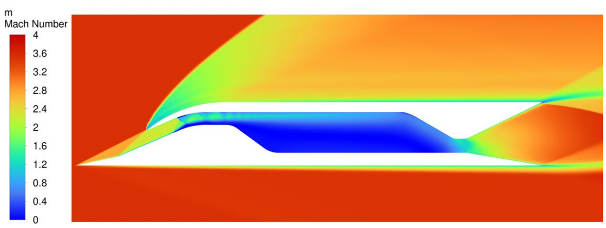

(a) Mach number

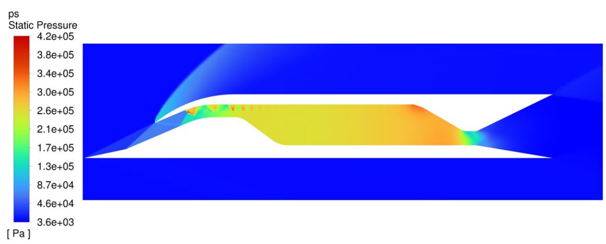

(b) Static pressure

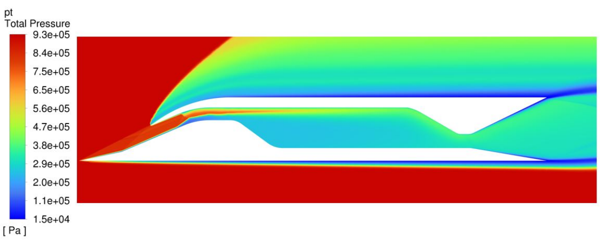

(c) Total pressure

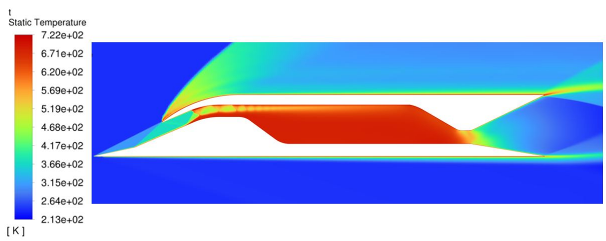

(d) Static temperature

Figure 6: Flow properties in the cold flow condition

DOI: 10.13009/EUCASS2025-365

4.3 Reactive Flow

The reactive flow simulations were carried out using species transport, volumetric reactions and turbulence-chemistry interaction through the eddy dissipation concept. This enabled the detailed modeling of the combustion process within the solid-fuel ramjet (SFRJ), where Hydroxyl-Terminated Polybutadiene (HTPB) was the fuel and atmospheric air the oxidizer.

HTPB can be generally described by the following structure:

$$\mathrm{HO{-}[CH_2{-}CH{=}CH{-}CH_2]}_n\mathrm{{-}OH}$$

Its thermal decomposition can thus be expressed as:

$$\mathrm{HO{-}[CH_2{-}CH{=}CH{-}CH_2]}_n\mathrm{{-}OH} \longrightarrow n\,\mathrm{C_4H_6} + 2\,\mathrm{OH} \tag{14}$$

- HO– and –OH are terminal hydroxyl groups.
- the $[CH_2–CH{=}CH–CH_2]_n$ is the repeating unit derived from 1,3-butadiene.
- n denotes the degree of polymerization, typically in the range 10–50.

which implies that HTPB decomposes predominantly into C_4H_6 units. Therefore, in this study, the combustion chemistry of HTPB was simplified by representing the fuel as C_4H_6, and a finite-rate chemistry model was adopted based on a reduced 2-step mechanism for HTPB-air combustion. This simplification is justified by the fact that C_4H_6 is the primary pyrolysis product of HTPB, allowing a good compromise between computational feasibility and physical accuracy, following the methodology proposed by Sankaran and validated against hybrid propulsion experiments.[10] The two-step global mechanism used was:

$$\mathrm{C_4H_6} + 3.5\,\mathrm{O_2} \rightarrow 4\,\mathrm{CO} + 3\,\mathrm{H_2O} \tag{15}$$

$$\mathrm{CO} + 0.5\,\mathrm{O_2} \leftrightarrow \mathrm{CO_2} \tag{16}$$

The Arrhenius parameters for these reactions were taken from the model described by J. A. Morinigo,[10] ensuring consistency with prior LES-based studies. The pyrolysis of HTPB was modeled as an inflow of 1,3-butadiene at the regressing fuel interface. The initial reactive simulations exhibited significant flow unsteadiness and instability, ultimately leading to an unstarted intake condition. As observed in the cold flow design phase, such phenomena are linked to choking at the nozzle throat. However, in this case, the cause is not simply the addition of fuel mass, but rather the heat release due to combustion. Combustion increases the total temperature (T_t) in the combustion chamber, which in turn reduces the maximum possible mass flow rate at the choked nozzle. The maximum choked flow rate for a perfect gas under isentropic conditions is given by:

$$\dot{m}_{\max} = A^* \cdot P_t \sqrt{\frac{\gamma}{RT_t}} \left(\frac{2}{\gamma+1}\right)^{\frac{\gamma+1}{2(\gamma-1)}} \tag{17}$$

where A^* is the nozzle throat area, P_t is the total pressure, T_t is the total temperature, R is the gas constant, and γ is the heat capacity ratio.

Due to the increase in T_t from combustion, $\dot{m}_{\max}$ decreases, potentially making the intake mass flow rate larger than the exhaust capacity of the nozzle. This imbalance leads to a progressive rise in chamber pressure until the two mass flow rates are equilibrated. The author identifies this phenomenon as a limitation driven by thermodynamic effects rather than by geometry. In particular, the temperature rise decreases the achievable mass flow rate through the nozzle, so that increasing the nozzle area becomes a practical solution. This effect was confirmed by iterative CFD simulations: in the first iteration, the flow choked and the intake unstarted. Only after increasing the nozzle throat area in the second iteration did the system reach stable steady state combustion.

DOI: 10.13009/EUCASS2025-365

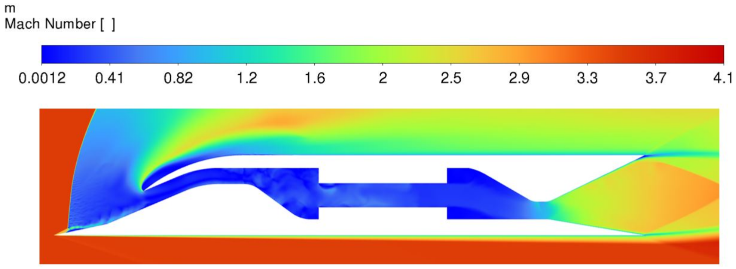

(a) Mach number - unstarted reactive case

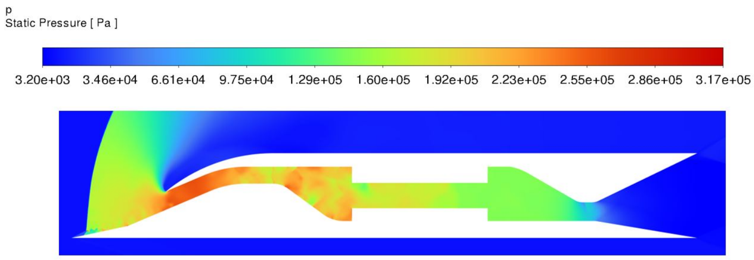

(b) Static pressure - unstarted reactive case

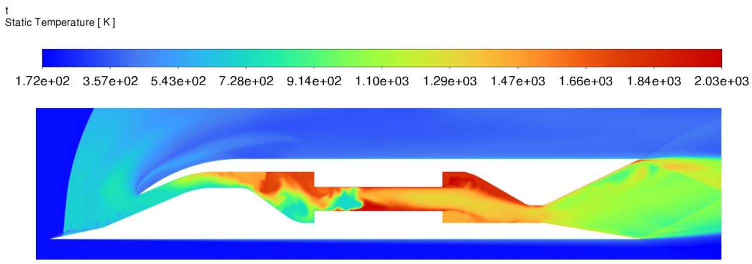

(c) Static temperature - unstarted reactive case

Figure 7: Flow properties in the unstarted reactive flow configuration.

Analyzing Figure 7a, the presence of a detached bow shock upstream of the intake is clearly visible. This is a direct indication of intake unstart, caused by a strong adverse pressure gradient that forces the normal shock system to move outside the isolator. As described previously, this phenomenon is typically triggered by excessive backpressure in the combustion chamber. This is further confirmed by Figure 7b, where the high static pressure distribution inside the combustion chamber can be clearly observed. The elevated chamber pressure exceeds the critical limit imposed by the intake geometry, destabilizing the shock train and leading to intake unstart. In Figure 7c, the combustion process results in strong thermal gradients that significantly increase the static temperature inside the chamber. As explained earlier, this rise in total temperature reduces the mass flow rate at the nozzle throat, effectively inducing intake unstarting. This mismatch between intake and outlet mass flow rates ultimately leads to the pressure buildup responsible for shock expulsion and unstart behavior.

DOI: 10.13009/EUCASS2025-365

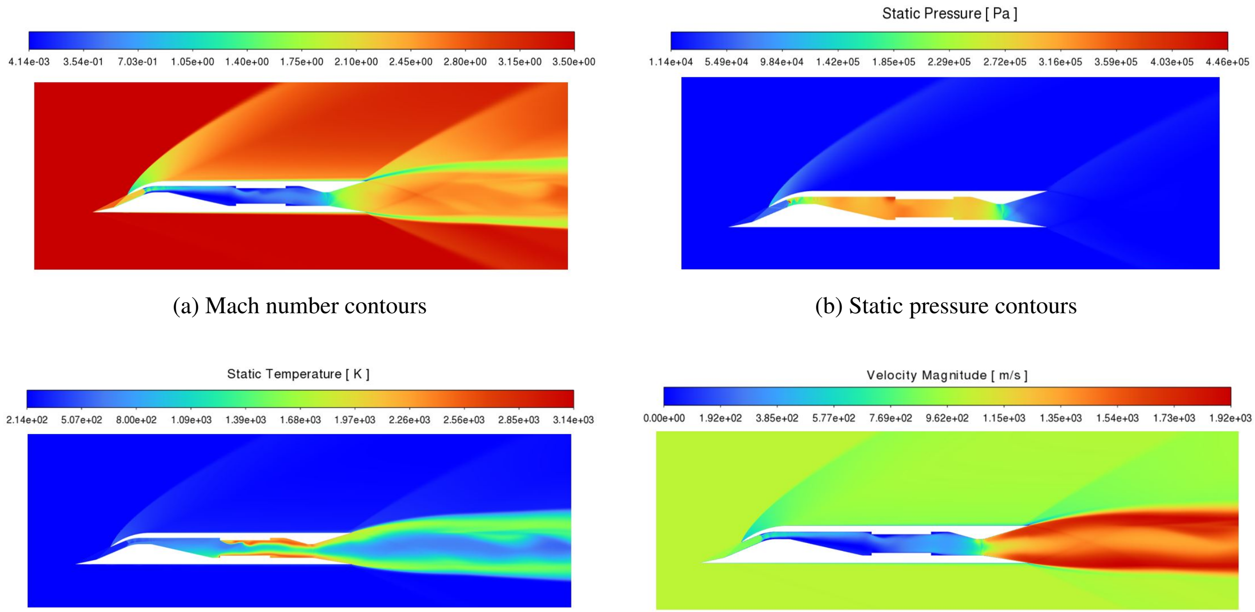

(a) Mach number contours

(b) Static pressure contours

(c) Static temperature contours

(d) Velocity contours

Figure 8: Flow field properties around the reactive region

Once the intake unstart issues were understood, further design improvements were implemented by including the thermal effects of combustion. Specifically, the final configuration accounts for the temperature rise due to combustion. Temperature was calculated by conducting a NASA CEA analysis of HTPB and air reaction products. The evaluated combustion chamber temperature, coupled with Eq. (17), was used to accurately estimate the nozzle throat area. It is critical to highlight that the temperature effects become relevant only when combustion occurs. Therefore, careful attention must be paid during the sizing process to ensure that the engine can operate safely in both reacting and non reacting conditions. In the absence of combustion, an oversized throat could cause the flow to remain too fast within the combustion chamber, leading to reduced residence time and poor ignition performance. While an ideal solution would involve a variable area nozzle, in this case a high temperature spark was simulated to reliably initiate the reaction and stabilize the flow. As shown in Fig. 8a, the normal shock is correctly located within the intake isolator, indicating proper shock positioning and flow deceleration. Figure 8b demonstrates a substantial pressure rise in the combustion chamber, confirming the successful establishment of the reacting regime. The combustion process leads to peak temperatures exceeding 3000 K, as displayed in Fig. 8c. While the itake and exit Mach numbers exhibit, as expected, only minor variations, the velocity plot in Fig. 8d clearly shows a strong acceleration downstream of the combustion chamber due to the heat release, which ultimately generates thrust. The mass fraction distributions offer additional insight into the quality of the combustion process. As shown in Fig. 9a, Fig. 9c, Fig. 9d, and Fig. 9e, the flow field is characterized by a high-speed core along the combustion chamber axis. This axial acceleration reduces the residence time and prevents uniform mixing, leading to an inhomogeneous distribution of key species. In particular, H_2O and CO primary products of the first combustion step are not evenly distributed, with higher concentrations confined to specific regions. The second reaction step produces CO_2, which appears more localized in hot spots where increased turbulence and residence time enhance reaction completion. These high CO_2 regions correspond to recirculation zones and stagnation pockets where the temperature remains elevated for longer durations. This behavior confirms the importance of local flow dynamics in driving secondary reaction kinetics.

Furthermore, the O_2 mass fraction remains non-zero throughout most of the chamber, indicating that the fuel rich core flow is surrounded by oxidizer rich regions. This stratification could be further exploited in future designs by introducing swirl or flame-holding mechanisms to enhance radial mixing and combustion efficiency.

DOI: 10.13009/EUCASS2025-365

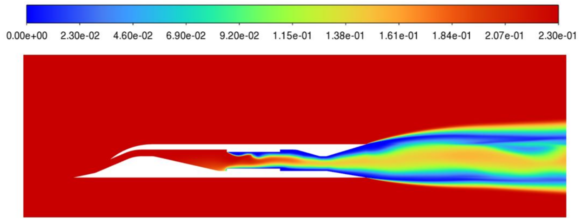

(a) O_2 mass fraction

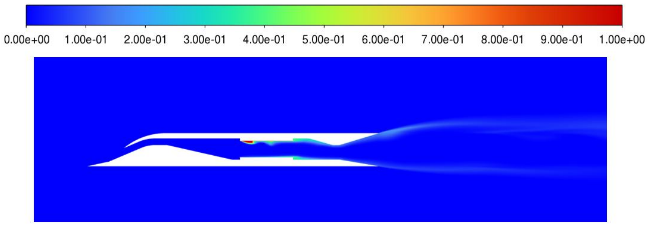

(b) C_4H_6 mass fraction

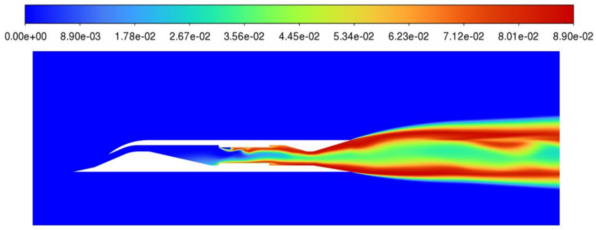

(c) H_2O mass fraction

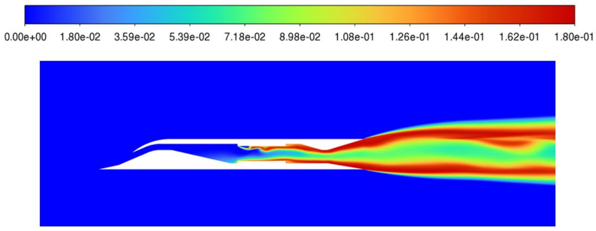

(d) CO mass fraction

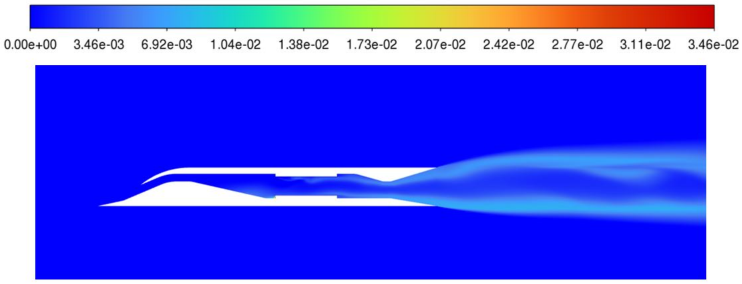

(e) CO_2 mass fraction

Figure 9: Mass fraction distributions of key species in the reacting flow

5. Conclusion

This study presents the complete design and optimization of a small scale solid fuel ramjet (SFRJ) intended for Mach 3.5 operation within a supersonic wind tunnel environment. Starting from the intake design, a novel efficiency metric was proposed to quantitatively balance total pressure recovery and aerodynamic drag, leading to an optimized two ramp mixed compression intake. The design was validated through CFD simulations, confirming the expected shock structure and deceleration profile. Following the intake, the combustion chamber and nozzle were developed with attention to fuel regression dynamics, O/F ratio constraints, and the need for flow stability under both cold and reactive conditions. The critical role of the nozzle throat sizing emerged from both theoretical and numerical analyses. Initial designs exhibited buzz instabilities and itake unstart behavior, attributed to a mismatch between intake and nozzle mass flow capacities. This phenomenon, driven by back pressure buildup, was mitigated by increasing the second throat area. The improved design demonstrated stable operation under cold flow conditions, and in reactive regime. The findings underscore the sensitivity of SFRJ systems to geometric balance especially in the presence of combustion induced thermal effects. The methodology presented here combining analytical modeling, empirical guidelines, and high fidelity CFD offers a robust framework for the development of compact, testable ramjet systems. The final configuration achieves the intended flow behavior and combustion conditions, providing a promising baseline for future testing and scaling to flight capable systems.

DOI: 10.13009/EUCASS2025-365

References

[1] F. Falempin. Ramjet and dual mode operation. In *Advances on Propulsion Technology for High-Speed Aircraft*, pages 7–1–7–36. RTO Educational Notes, RTO-EN-AVT-150, 2008.

[2] S. Krishnan and P. George. Solid fuel ramjet combustor design. *Progress in Aerospace Sciences*, 34:219–256, 1998.

[3] D. G. Fletcher. Fundamentals of hypersonic flow - aerothermodynamics. In *RTO-EN-AVT-116*, 2004. Lecture Series at the von Karman Institute, Belgium.

[4] J. D. Anderson. *Modern Compressible Flow: With Historical Perspective*. McGraw-Hill Education, New York, NY, 3 edition, 2002.

[5] S. F. Hoerner. *Fluid-Dynamic Drag*. Hoerner Fluid Dynamics, Brick Town, New Jersey, 1965.

[6] J. P. S. Sandhu, M. Bhardwaj, N. Ananthkrishnan, A. Sharma, J. W. Park, and I. S. Park. Tradeoffs in biconic intake aerodynamic design optimization with sub-optimal oswatitsch solutions. Technical report, Yanxiki Tech and Agency for Defense Development, 2025.

[7] J. Seddon and E. L. Goldsmith. *Intake Aerodynamics*. AIAA Education Series. American Institute of Aeronautics and Astronautics, Reston, VA, 2 edition, 1999.

[8] T. Cain. Ramjet intakes. Rto-en-avt-185, NATO Research and Technology Organisation, 2010.

[9] R. Nicoletti, F. Margani, L. Armani, A. Ingenito, C. Fujio, H. Ogawa, S. Han, and B. J. Lee. Numerical investigation of a supersonic wind tunnel diffuser optimization. *Aerospace*, 12(5):366, 2025.

[10] J. A. Morinigo and J. Hermida-Quesada. Evaluation of reduced-order kinetic models for htpb-oxygen combustion using les. *Aerospace Science and Technology*, 58:358–368, 2016.